

Hamiltonian learning quantum magnets with non-local impurity tomography

Greta Lupi¹ and Jose L. Lado¹

¹*Department of Applied Physics, Aalto University, 02150 Espoo, Finland*

(Dated: December 11, 2024)

Impurities in quantum materials have provided successful strategies for learning properties of complex states, ranging from unconventional superconductors to topological insulators. In quantum magnetism, inferring the Hamiltonian of an engineered system becomes a challenging open problem in the presence of complex interactions. Here we show how a supervised machine-learning technique can be used to infer Hamiltonian parameters from atomically engineered quantum magnets by inferring fluctuations of the ground states due to the presence of impurities. We demonstrate our methodology both with a fermionic model with spin-orbit coupling, as well as with many-body spin models with long-range exchange and anisotropic exchange interactions. We show that our approach enables performing Hamiltonian extraction in the presence of significant noise, providing a strategy to perform Hamiltonian learning with experimental observables in atomic-scale quantum magnets. Our results establish a strategy to perform Hamiltonian learning by exploiting the impact of impurities in complex quantum many-body states.

I. INTRODUCTION

Quantum magnetism provides a highly flexible playground to engineer exotic phenomena [1, 2]. While a variety of natural materials host frustrated and magnetic states, accessing the most unconventional regimes often requires using artificial platform where Hamiltonians can be engineered [3]. Atomic-scale quantum magnets [4–11] have opened new avenues for exploring fundamental quantum phenomena, enabling controllable platform to engineer symmetry breaking [12], quantum criticality [13], emergent excitations [14, 15], and topological states [16, 17]. Scanning tunneling microscopy (STM) enables creating and probing artificial quantum states with high spatial and energy resolution, providing detailed insights into the behavior of quantum magnets [4–11, 18, 19]. Electrically driven paramagnetic resonance with STM have brought quantum control at the atomic scale to remarkable levels. ESR-STM enabling energy resolution several orders of magnitude below thermal noise [10, 20], allowed quantum gate at the atomic level [21], and probing time evolution of magnetic dynamics with atomic accuracy [22]. Single atom manipulation in quantum magnet thus enables a degree of control radically different than in bulk materials, motivating the development of new strategies to tackle open problems in quantum magnetism [23].

Understanding an experimental quantum many-body systems relies on having an accurate description of the many-body interactions. Traditional methods of determining Hamiltonian parameters often rely on fitting experimental data to theoretical models. Characterizing quantum spin liquids represents a remarkable problem in quantum materials [1, 2] due to the intricate nature of its ground state, and often requiring new strategies to find their experimental signatures [24–30]. As a result, even in relatively simple quantum magnets, determining the Hamiltonian from experimental data can be remarkably difficult [3]. Machine learning provides a flexible strategy to enable learning of Hamiltonian parameters

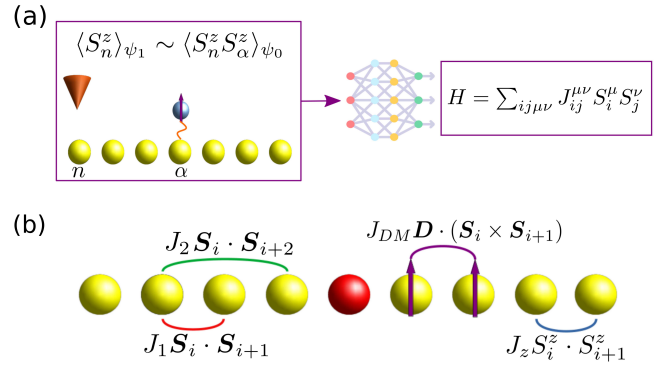


FIG. 1. (a) Schematic representation of the Hamiltonian learning strategy that leverages the response of a quantum magnet to perturbations. The inclusion of perturbations in a quantum magnet provides access to the non-local correlator, that enables learning the original quantum many-body Hamiltonian. (b) Shows the specific quantum magnet we will focus on, featuring first and second neighbor exchange, anisotropic exchange and Dzyaloshinskii-Moriya interaction.

directly from physical observables [23, 31–34]. Hamiltonian learning can be done with data generated from theoretical models, that can be later on directly applied to experimental measurements [35, 36]. This strategy leverages the exceptional ability of machine learning methods to identify non-trivial correlations in observables that enable extracting information about the underlying ground state and Hamiltonian [37–48].

Here we show how the Hamiltonian of a quantum magnet can be directly inferred from measurements of the response of the spin chain to individual impurities. Our strategy relies on using the response of the system to extract the Hamiltonian using a machine learning strategy. The inclusion of individual impurities create a perturbation in the ground state that directly reflects the underlying Hamiltonian, a correlation that can be mapped with a supervised neural network. We show

that this methodology enables extracting long range and anisotropic exchange interactions, often a challenge to infer in experiments. We show that this methodology can be understood as a generalization of Hamiltonian extraction in a fermionic model, a procedure that it is often performed in STM via quasiparticle interference. Our manuscript is organized as follows. In Section II we describe the experimental strategy to obtain the data required for our Hamiltonian extraction. Section III details the many-body spin models we study, including the fermionic version that provides a minimal exemplification of our methodology. The methods employed for Hamiltonian parameter extraction using neural networks are described in Section IV, where we discuss the training process, data generation, and the inclusion of noise to simulate experimental conditions. In Section V, we present the results of the Hamiltonian inference, demonstrating the resilience of our methodology to noise both in the evaluation as well as during training. Finally, in Section VI, we summarize our conclusions.

II. IMPURITY PERTURBATIONS AND NON-LOCAL RESPONSE

Our methodology will rely on using the non-local response of the system to extract the Hamiltonian. However, STM measures local quantities rather than non-local ones, and thus first an strategy must be developed to extract the required non-local information. Non-local correlators of quantum spin chain determine the response of the quantum many-body system to perturbation in the sites, and thus are reflected when adding additional impurities that act as exchange sources. Specifically, additional sites featuring strong single ion anisotropy as local perturbations, which then enable to measure elsewhere in the system what is the change they created to the ground state. Experimentally, this was demonstrated with dysprosium single atom magnets [49], enabling atomic-scale magnetic field with stabilities above days. The Dy impurity creates a local exchange field in the neighboring site, which as a result modified the expectation value of the magnetization in the rest the system. This strategy is exemplified in Fig. 1a.

The relationship between the response to local perturbations and non-local correlators can be rationalized via Kubo formalism [50]. In the following we will consider two Hamiltonians H_1 and H_0 , where H_1 is a perturbed Hamiltonian, and H_0 the Hamiltonian without perturbation. For the sake of concreteness, we will consider a local perturbation consisting on a local time-dependent exchange field in site α , with the full Hamiltonian taking the form

$$H = \sum_{ij} J_{ij} \mathbf{S}_i \cdot \mathbf{S}_j + B_\alpha^z(t) S_\alpha^z = H_0 + V(t) \quad (1)$$

using time-dependent perturbation theory in the Heisenberg picture, the change of the expectation value of the

magnetization in site n takes the form [51]

$$\delta \langle \hat{S}_n(t) \rangle = \int_{-\infty}^{\infty} \chi_{\alpha,n}(t,t') B_\alpha^z(t') dt \quad (2)$$

where $\chi_{\alpha,n}(t-t')$ is the non-local time-dependent spin-spin response that can be computed with Kubo formalism [50, 52, 53] as

$$\chi_{\alpha,n}(t-t') = -i\theta(t-t') \langle [\hat{S}_n^z(t), \hat{S}_\alpha^z(t')] \rangle \quad (3)$$

where $\hat{S}_n^z(t)$ are the spin operators in the Heisenberg picture, and θ the step function. The previous relationship shows that the change in the expectation value of the magnetization in site n when a perturbation is added in site α is given by the non-local two-point spin-spin correlator. This highlights that time-dependent measurements in magnetic spin chains directly reflect the time-dependent two-point spin correlations of the quantum magnet ground state.

The relationship between response to a local impurity and the non-local spin-spin correlator becomes specially transparent in the limit of a time-independent perturbation and a strong many-body gap. We will consider a system whose spectra has a typical gap between ground state and excited states Δ . We take that the ground state ψ_0 denote the ground state of H_0 , the system without the external source, and ψ_1 the ground state of $H_1 = H_0 + V$, the system with the local time-independent source, which can be realized by adding an Ising Dy site to the quantum magnet. Taking the perturbation $V = B_\alpha^z S_\alpha^z$, the correction in the expectation value of the local magnetization at site n , $\langle S_n^z \rangle_{\psi_1}$ can be expressed with second order perturbation theory as

$$\langle S_n^z \rangle_{\psi_1} \approx B_\alpha^z \sum_{\nu} f(\epsilon_\nu) \langle \psi_0 | S_n^z | \Psi_\nu \rangle \langle \Psi_\nu | S_\alpha^z | \psi_0 \rangle + \text{h.c.}, \quad (4)$$

where we take $\langle S_n^z \rangle_{\psi_0} = 0$ for the unperturbed expectation value for a quantum magnet, $|\Psi_\nu\rangle$ represents the excited states of the unperturbed Hamiltonian, $f(\epsilon_\nu) = 1/\epsilon_\nu$ is the prefactor stemming from perturbation theory, where ϵ_ν is the energy difference between the ground state $|\psi_0\rangle$ and excited states $|\Psi_\nu\rangle$ of H_0 . It worth noting that Eq. 4 is obtained by taking the spectral representation of the Kubo formula Eq. 2 and Eq. 3 in the static limit. The contributions from excited states that give rise to a finite contribution in Eq. 4 stem from low energy states featuring excitations over the ground state that link sites α and n . Taking that the relevant energy scales of the excitations that correct the original ground state is $\Delta = \langle \epsilon_\nu \rangle$, we can make the replacement in Eq. 4 $\sum_{\nu} f(\epsilon_\nu) |\Psi_\nu\rangle \langle \Psi_\nu| \sim \frac{1}{\Delta} \mathcal{I}$. This allows to rewrite the correction to the magnetization as

$$\langle S_n^z \rangle_{\psi_1} \sim \frac{B_\alpha^z}{\Delta} \langle S_n^z \cdot S_\alpha^z \rangle_{\psi_0}. \quad (5)$$

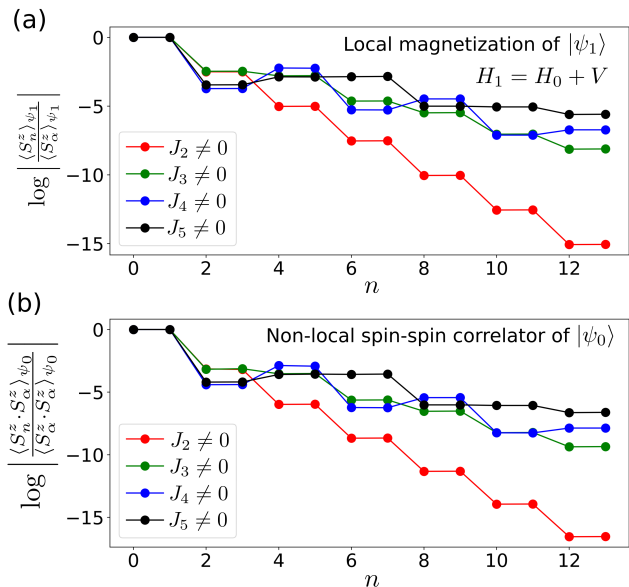


FIG. 2. Comparison between (a) the magnetization of a quantum spin chain of Eq. 7 in the perturbed state ψ_1 , with the Ising Dy source coupled at site $\alpha = 0$, and (b) the non-local static correlator of the same spin chain in the unperturbed state ψ_0 . It is observed that both local magnetization and non-local correlator feature analogous site dependence, and in particular strongly changing depending on the additional long range exchange coupling included. We took $\delta = 0.9$, $J_k = 0.2J_0$ and $B_\alpha^z = 0.01J_0$.

To factor out the dependence on the strength of the perturbation, the previous result can be normalized by the perturbed magnetization and unperturbed correlators in site α , giving rise to

$$\frac{\langle S_n^z \rangle_{\psi_1}}{\langle S_\alpha^z \rangle_{\psi_1}} \approx \frac{\langle S_n^z \cdot S_\alpha^z \rangle_{\psi_0}}{\langle S_\alpha^z \cdot S_\alpha^z \rangle_{\psi_0}} \quad (6)$$

This relationship allows us to connect the local magnetization $\langle S_n^z \rangle_{\psi_1}$ for a gapped static system, which is experimentally measured via the differential conductance $\frac{dI}{dV}$ using spin polarized STM, to the non-local spin correlator $\langle S_n^z \cdot S_\alpha^z \rangle_{\psi_0}$ in the unperturbed system. We illustrate the comparison between these quantities in Figure 2. For the sake of concreteness, we take a Hamiltonian with long-range exchange interaction and dimerization taking the form $H = H_0 + V$, where

$$H_0 = \sum_n J_1 (1 + \delta(-1)^n) \mathbf{S}_n \cdot \mathbf{S}_n + \sum_{k=2}^5 \sum_n J_k \mathbf{S}_n \cdot \mathbf{S}_{n+k} \quad (7)$$

, which features a many-body gap for $\delta \neq 0$ and $J_k \ll J_1$ for $k = 2, 3, 4, 5$. Figure 2a shows the magnetization in the different sites upon adding the local exchange perturbation, whereas Figure 2b shows the non-local spin-spin

correlator in the absence of perturbation. It is clearly observed that both quantities feature very good correspondence over several orders of magnitude, which allows to infer non-local correlators from measuring local magnetizations of perturbed quantum magnet. The system features a decay correlation and magnetization for all the different couplings considered, yet interestingly the type of long range coupling included dramatically changes the speed of the decay and the oscillations. In this fashion, even though all those system feature similar many-body gaps, the magnetization and correlators provide a strong fingerprint of the underlying Hamiltonian. These unique behavior for the different coupling parameters is what provides the starting ground to attempt Hamiltonian learning from the observables in Figure 2.

The previous methodology exemplifies how non-local spin correlations can be extracted from local STM measurements by engineering local magnetic sites [4–6, 54]. As a result, Hamiltonian learning could be performed either directly by measuring the local response a system when adding local perturbations on different sites (Fig. 2a), or with the non-local correlator in the unperturbed limit (Fig. 2b). It is worth noting that this strategy can be also used for single particle systems, just by replacing the spin operators by fermionic operators and adapting the Kubo formalism accordingly. In terms of Hamiltonian learning, we will illustrate both single particle and the quantum many-body magnet cases. For the sake of concreteness, we will perform Hamiltonian learning with local measurements of perturbed systems for the fermionic case, and with the non-local correlators for the quantum many-body limit, yet noting that either local perturbed measurements or non-local unperturbed measurements allow for Hamiltonian learning in both cases. It is finally worth noting that time-dependent measurements, either local or non-local, could be used for Hamiltonian learning [55–64].

III. MODELS

In this section, we introduce the two systems where we demonstrate our methodology, a fermionic chain and a quantum many-body spin-1/2 chain. The fermionic chain represents a single-particle model, and it allows us to demonstrate our methodology as a generalization of Hamiltonian extraction with quasiparticle interference. Beyond its application on a conventional metal, it is worth noting that a single particle Hamiltonian learning could be performed as a quasiparticle description of a quantum magnet in terms of auxiliary spinons. The quantum many-body spin chain solved with tensor network methods represents the more accurate and challenging case, and is the case where methodology demonstrates its potential. In this case, we compute the exact quantum many-body ground and required expectation values using the full quantum many-body wavefunction using tensor networks

A. Fermionic chain with a magnetic impurity

We start by considering a single particle model for which we will later perform Hamiltonian learning. While the single particle case is much simpler than the many-body model, it will allow us to exemplify the essence of Hamiltonian learning with non-impurity tomography that we will later exploit in the quantum many-body case. The fermionic Hamiltonian that we consider takes the form:

$$H = t_1 \sum_{i=1}^{n-1} c_i^\dagger c_{i+1} + t_2 \sum_{i=1}^{n-2} c_i^\dagger c_{i+2} + \quad (8)$$

$$+ \mu \sum_{i=1}^n c_i^\dagger c_i + i\lambda_R \sum_{i=1}^{n-1} [\hat{z} \times (\mathbf{r}_i - \mathbf{r}_{i+1})] \cdot \boldsymbol{\sigma} c_{i,s}^\dagger c_{i+1,s'},$$

where t_1 and t_2 are the nearest-neighbor and next-nearest-neighbor hopping parameters, respectively, μ is the chemical potential, and λ_R represents the strength of the Rashba SOC [65–67]. Here, c_i^\dagger and c_i are the creation and annihilation operators at site i , \mathbf{r}_i is the position vector at site i , $\boldsymbol{\sigma}$ are the Pauli matrices representing the spin degrees of freedom, and s and s' denote the spin indices. The term $[\hat{z} \times (\mathbf{r}_i - \mathbf{r}_{i+1})] \cdot \boldsymbol{\sigma}$ captures the spin-orbit interaction arising from the presence of a magnetic impurity.

We modeled the fermionic chain with a magnetic impurity positioned at the center, coupled to the chain with a strength of $\delta = 0.4$. We consider an infinite system that we solve exactly using a Green's function embedding algorithm. The observable that will be used as input of the machine learning algorithm is the local spectral function of the perturbed system, defined as

$$A(n, \omega) = \sum_s \langle \Omega(\omega) | c_{n,s} \delta(\omega - H) c_{n,s}^\dagger | \Omega(\omega) \rangle, \quad (9)$$

where s denotes the spin and $|\Omega(\omega)\rangle$ is the ground state of the system at the frequency ω . The previous quantity corresponds to the local density of states in the presence of an impurity. The local impurity gives rise to scattering of the conduction electrons, that create oscillations of the density of states. Such oscillations are a direct consequence of the electronic dispersion of the system, and reflect the scattering wavevectors associated to the band structure. This phenomenology is directly used in quasiparticle interference to infer Fermi wavevectors from experimental data. In particular, the Fourier transform of the density of states fluctuations reflects a self-convolution of the electronic structure. We will train a machine algorithm that allows to directly infer the parameters of the Hamiltonian from the spectral function and its Fourier transform.

B. Quantum spin 1/2 model with a spin-1 impurity

The second system that we will consider is a full quantum many-body model, consisting on a spin-1/2 chain with long range exchange and anisotropic interactions. The Hamiltonian of the spin chain is defined as:

$$H = J_1 \sum_{i=1}^{n-1} \mathbf{S}_i \cdot \mathbf{S}_{i+1} + J_2 \sum_{i=1}^{n-2} \mathbf{S}_i \cdot \mathbf{S}_{i+2} + \quad (10)$$

$$+ J_z \sum_{i=1}^n S_i^z \cdot S_{i+1}^z + J_{DM} \sum_{i=1}^{n-1} \mathbf{D} \cdot (\mathbf{S}_i \times \mathbf{S}_{i+1})$$

$$+ B^z \sum_{i=1}^n S_i^z + B^x \sum_{i=1}^n S_i^x,$$

where J_1 and J_2 represent the nearest-neighbor and next-nearest-neighbor exchange interactions, J_z is the anisotropic exchange interaction, J_{DM} denotes the Dzyaloshinskii-Moriya (DM) interaction [68, 69] with \mathbf{D} as the DM vector (which we take with module equal to 1), and B^z and B^x is an external tunable magnetic field that acts along the z and x -direction, perpendicular and parallel to the plane in which the chain lies. Our Hamiltonian learning strategy requires two different types of atoms, the ones forming the quantum magnet, and the Ising magnetic field source. In order to amplify the effect of the perturbation, it is however fitting to consider we include a $S = 1$ site in the middle, denoted as the amplifier site in Fig. 1c. This site leads to a finite local spin susceptible to yield a large response in the presence of the proximity to the Ising Dy source. While extracting the response of the system does not require having the $S = 1$ site, we will include in the following to demonstrate that the strategy works in this experimentally relevant case. The external magnetic field B^z in the model enables controlling the ground state of the system [70], and will provide the parameter enabling Hamiltonian inference. In the absence of an external magnetic field, the Hamiltonian features time-reversal symmetry, but broken rotational symmetry due to the anisotropic exchange terms. It is worth considering two limiting cases in which the non-local correlators would feature dramatically different behavior. In the limiting case where only J_1 is non-zero, the ground state features quantum disorder and realizes a pristine $S = 1/2$ Heisenberg model featuring gapless spinons that give rise to non-local correlations featuring a power-law decay. In stark contrast, if only J_z is non-zero, the Hamiltonian realizes an Ising model, that features a ground state with stagger magnetization, with leads to an oscillating $\langle S_n^z S_\alpha^z \rangle$ correlator. By including a spin-1 impurity, we introduce localized magnetic interactions that perturb the system, offering insights into how impurities affect quantum correlations and the overall ground state.

The object that we will use for Hamiltonian learning is the field-dependent non-local correlator, defined as

$$\chi(n, B_z) = \langle \Omega(B_z) | S_n^z S_\alpha^z | \Omega(B_z) \rangle, \quad (11)$$

where $|\Omega(B_z)\rangle$ is the ground state of the system at field B_z , S_i^z is the z -component of the spin operator at site n , and S_α^z is the z -component of the spin operator at the impurity site α . This observable is related to the response of the system to local Ising impurities as described in Sec. II, and in the gapped limit is given directly by the magnetization in the presence of a perturbation as shown in Eq. 6. We use the static correlator with respect to the impurity in the middle of the chain, where we considered chains with $L = 21$ sites, with the central site the $S = 1$ site.

IV. METHODS

In this section, we present the methodologies employed in our study to explore Hamiltonian learning using machine learning techniques.

A. Hamiltonian Learning with neural networks

Our objective is to develop an algorithm capable of mapping the field-dependent non-local correlators to the Hamiltonian of the system. While the inverse step can be performed systematically with a quantum many-body solver, extracting the Hamiltonian from observables requires an alternative strategy. We use a machine learning methodology based on supervised learning for this purpose, for which a training set with Hamiltonians and non-local correlators is required. In Hamiltonian learning, the targets are specifically the parameters of the Hamiltonian that define the interactions within the system. The Hamiltonian we will study take the general form of

$$H = \sum_n \Lambda_n \mathcal{H}_n \quad (12)$$

where \mathcal{H}_n represents the interaction terms with their corresponding parameters Λ_n . This approach allows us to easily add or remove interactions from our model as needed. The targets, or the parameters Λ_n , are initially sampled uniformly within a specific range. This range is carefully chosen to avoid crossing any phase transitions, ensuring the stability and accuracy of our model. After feeding the NN with both input data and targets, the model should be trained and ready to make predictions on a brand new test set of data.

We start with the one-dimensional electron gas interacting sites with an impurity (Fig. 1b). The presence of scatterers allows us to probe the response of the system to perturbations, leading to frequency and spatial features that the NN leverages to extract the Hamiltonian. We consider first and second neighbour interactions between the sites and, most importantly, the spin-orbit coupling (SOC). SOC terms present significant challenges for NN learning due to their intrinsic complexity. These terms involve non-linear and anisotropic interactions between

spin and orbital angular momentum, increasing the dimensionality of the problem. Additionally, SOC effects are highly dependent on the system's symmetry, making generalization difficult for the NN. The introduction of SOC also leads to complex electron correlation effects, which are not easily captured by NNs.

After a first training of the NN with perfect theoretical data, we performed a re-training with noisy data incorporating magnetic noise. This approach ensures that the trained models can effectively handle and make accurate predictions even when confronted with experimental data featuring magnetic noise, a crucial requirement for their application in practical quantum systems.

B. Neural Network Architecture

For the fermionic chain system, we employed a fully connected NN architecture. The physically meaningful quantity used as input to train the network is the spectral function, as defined in Section III A. We generated a dataset of 5000 samples, with 3000 samples designated for training and 1000 samples for testing. The training process spanned around 100 epochs, utilizing a batch size of 32. The Adam optimizer was used for optimization, with a learning rate set to 10^{-4} . The input data for the NN was prepared by considering a chain of 150 sites. We evaluated the spectral function for three different voltage biases, $V \in [-0.5, 0, 0.5]$, and then applied a Fourier transform to the spectral function data. This preprocessing step resulted in an input size of 900 for the first layer of the NN. The loss function used for training was the mean squared error (MSE). The chosen parameter ranges are as follows: μ and λ_R ranged from $[0, 1]$, while t_2 spanned $[0, 2]$. The workflow of our NN training for the fermionic chain is illustrated in Fig. 4a. Magnetic noise at levels of $\Delta_B = 0.05$ and $\Delta_B = 0.1$ was added to the original data, and these noisy datasets were used to fine-tune the NN for an additional 50 epochs.

For the spin chain system we employed a fully connected NN architecture. Here, we exploited the static spin correlator as input to train the NN, as defined in Section III B. We generated a dataset of 2000 samples, with 1200 samples for training and 400 samples for testing. The training process employed 200 epochs, utilizing the Adam optimizer with a learning rate of 10^{-4} . The input data for the NN was prepared by considering a chain of 21 sites. We evaluated the static spin correlator for 12 different external magnetic fields in the range $B \in [0, 5]$, resulting in an initial input size of 252. We then applied Principal Component Analysis (PCA) to reduce the input size to 200 components. The loss function used for training was the mean squared error (MSE). The parameter ranges selected for the spin chain study are J_2 and J_z ranging from $[-0.5, 0.5]$, and J_{DM} spanning $[0, 1]$. The workflow of our algorithm for the spin chain is illustrated in Fig. 6a. After the initial training, we added magnetic noise at levels of $\Delta_B = 0.05$ and $\Delta_B = 0.1$ to the original

data. These noisy datasets were used to fine-tune the NN for an additional 50 epochs.

C. Fidelity Evaluation

To assess the robustness of the NN training against noise, we define fidelity using the Pearson correlation coefficient [34, 71, 72]:

$$\mathcal{F}_{\Lambda_n} = \frac{\langle \Lambda_n^{\text{pred}} \Lambda_n^{\text{true}} \rangle - \langle \Lambda_n^{\text{pred}} \rangle \langle \Lambda_n^{\text{true}} \rangle}{\sqrt{\text{var}(\Lambda_n^{\text{pred}})} \sqrt{\text{var}(\Lambda_n^{\text{true}})}}, \quad (13)$$

where X_{pred} represents the predicted values, X_{true} represents the true values, and $\text{var}(\cdot)$ denotes the variance. The fidelity quantifies the correlation between the predicted and true values, thereby evaluating the NN's performance under noisy conditions. The fidelity, \mathcal{F} , is defined on the interval $[0, 1]$, where $\mathcal{F} = 1$ indicates perfect prediction accuracy, implying $\Lambda_{\text{pred}} = \Lambda_{\text{true}}$, while $\mathcal{F} = 0$ corresponds to no predictive accuracy.

D. Noise models

A crucial aspect of Hamiltonian learning is its robustness in scenarios where the observables feature noise. In the following we will consider two different sources of noise. The first source consist on magnetic noise, meaning a fluctuating background magnetic field that affects all the local magnetization measured. This first noise source adds a typical random value to each correlator, and may flip its sign in certain cases. Experimentally, this type of noise contribution may arise from residual fluctuating magnetic fields with a time scale slower than the measurement time [73–75]. A second source can be an offset created by the magnetic field of the tip used in scanning tunneling microscopy during the measurement of the local magnetization of the sites [76–79]. From a theoretical perspective, this type of noise expectation values can also emerge in many-body calculations in case the ground states are not computed with enough accuracy, which in the case of matrix product states would arise from using a not sufficiently large bond dimension [80]. The second type of noise is denoted as scaling noise, which it does not necessarily change the sign of the magnetization measured, but rather impacts its magnitude. This type of noise would arise from uncertainties on the value of the magnetization when using a second atom as detector [81–83], allowing to measure relative changes in the magnetization can be observed, but the estimation of the absolute value may show fluctuations. From the perspective of the non-local correlators, the two noise models are included as follows.

Magnetic noise is included by adding a background contribution to the measured moments as

$$\langle S_\alpha^z S_n^z \rangle_{\text{MagNoise}} = \langle S_\alpha^z S_n^z \rangle + \mathcal{N}(\Delta_B^2), \quad (14)$$

where $\langle S_\alpha^z S_n^z \rangle$ represents the original data for the i -th instance and $\mathcal{N}(0, \sigma^2)$ is the Gaussian noise with zero average and standard deviation Δ_B^2 . This type of noise specially impacts long-range correlations, and in particular limits the accuracy of the potentially extracted correlation length of the quantum many-body state. In contrast, short range correlations will be much less affected than long-range ones due to its substantially larger value.

The scaling noise takes the form

$$\langle S_\alpha^z S_n^z \rangle_{\text{ScaNoise}} = \langle S_\alpha^z S_n^z \rangle (1 + W(n_s)), \quad (15)$$

where n_s is a random variable uniformly distributed between -0.5 and 0.5 . This noise specially impacts the quantitative values of short range correlations. In contrast, extracted correlation length of the quantum many-body state, that depends on the decay of long range correlations, are relatively robust to this perturbation.

We include this two noise sources at two different levels in our methodology. The magnetic noise of Eq. 14 is included directly in the input data used in retraining the model, and would account both for experimental residual magnetic noise, and computational inaccuracies of a quantum many-body solver. The scaling measurement noise of Eq. 15 is included only when testing the robustness of the fully trained algorithm, and would account for uncertainties in the measured magnetic moment due fluctuation current onsets. In the case of the single particle model, noise is included with analogous functional forms, where the role of magnetic noise is replaced by electronic noise measured in the spectroscopy [84], and scaling noise stems from potential fluctuations in the set-point current [85].

V. NOISY HAMILTONIAN LEARNING

In this section, we investigate the impact of noise on Hamiltonian learning. While computational calculations do not feature the same sources of noise as experimental ones, the solution of quantum many-body systems may feature numerical noise to the the approximate nature of the many-body methods. This is specially relevant in the case of tensor-network states, where the bond dimension of the variational algorithm determines the accuracy of the ground state. By examining how noise affects the accuracy and stability of Hamiltonian reconstruction, we can better understand the limitations and potential optimizations of machine learning methods in quantum systems.

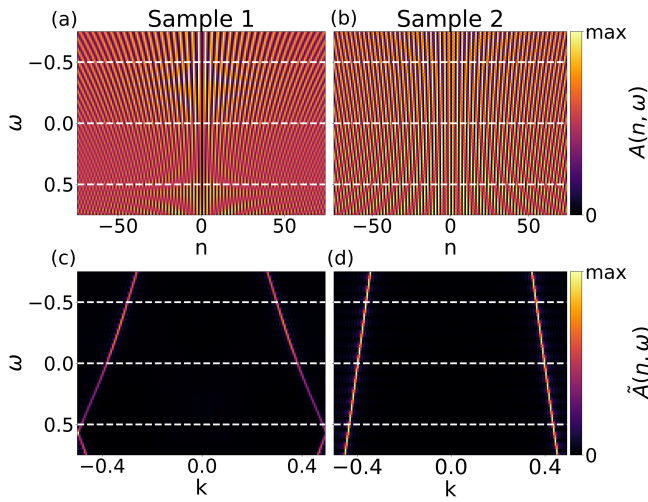


FIG. 3. Evolution of the spectral function of two different infinite electronic system (a,c) and (b,d) with a magnetic impurity. Panel (a,b) shows the spectral function in real space $A(n, \omega)$ and panels (c,d) its Fourier transform $\tilde{A}(k, \omega)$, as a function of the frequency ω and, respectively, the position in real-space and momentum-space. The different features that appear in each pair (a,c) and (b,d) enables extracting the original Hamiltonian.

A. Single-particle system

The spectral function provides information about the electronic structure of the system at different energy levels. By training the NN with the spectral function data, both in real space and its Fourier transform, we can extract essential features and parameters of the Hamiltonian. Fig. 3 shows how the spectral function and its Fourier transform evolve with different biases, in real and momentum space. This problem is fundamentally an image recognition task, where the NN is trained to recognize patterns in the spectral function and Fourier spectral function plots. The Fourier spectral function enables augmenting the input data, which is specially useful to extract the subtlety of the Rashba SOC effects. The Rashba coupling introduces a spin-dependent interaction that is often very subtle and difficult to detect directly from the spectral in real space. In fact, Rashba effect can create small shifts and splittings in the electronic structure that might not be easily discernible in real-space DOS plots [66]. By transforming the spectral function data into momentum space, these subtle effects become easier to extract for the machine learning algorithm. This is because the SOC influences the relative distances between peaks in the Fourier transform, making these interactions more detectable. By training the machine learning algorithm with these simulations, we obtain an algorithm capable of inferring the Hamiltonian parameters from the local observables.

Fig. 4b shows the fidelity of the extracted Hamiltonian parameters μ , t_2 , and λ_R as a function of the noise

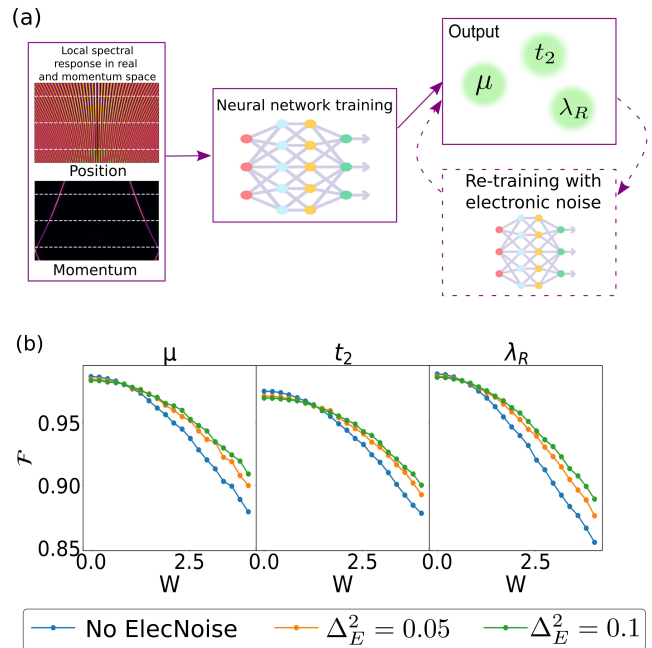


FIG. 4. (a) Workflow for the fermionic model. Panel (b) shows the fidelity of the fermionic chain model parameters μ , t_2 , and λ_R as a function of the scaling measurement noise W . Each plot compares the fidelity for data without magnetic electronic ($\Delta_E^2 = 0$) and with electronic noise levels $\Delta_E^2 = 0.05$ and $\Delta_E^2 = 0.1$.

level w . The plots compare the fidelity for perfect data, $\Delta_E^2 = 0.05$, and $\Delta_E^2 = 0.1$ electric noise levels. As expected, the fidelity shows a gradual decline with increasing magnetic noise. For μ , the model demonstrates high robustness, maintaining a fidelity close to 0.9 even with electric noise $\Delta_E^2 = 0.1$ at scaling noise of $W = 2$. The fidelity for t_2 also declines with increasing W but remains quite high overall, with a noticeable drop beyond $W = 3$. The fidelity for λ_R is similarly robust, showing a gradual decrease with higher noise levels and maintaining a relatively high fidelity even at with electric noise $\Delta_E^2 = 0.1$.

B. Hamiltonian learning a many-body quantum spin model

We now move to consider the spin quantum many-body Hamiltonian and extract its parameters from the non-local correlators. In the single particle case, the change in chemical potential allow extracting information of the non-local correlators for a ground-state-dependent state. For the quantum spin model a chemical potential is however not present, and its role is replaced by an external magnetic field. The tunability of the magnetic field B in the Hamiltonian allows us to use the static spin correlator as training data for the NN, and its change with the magnetic field provides the non-trivial

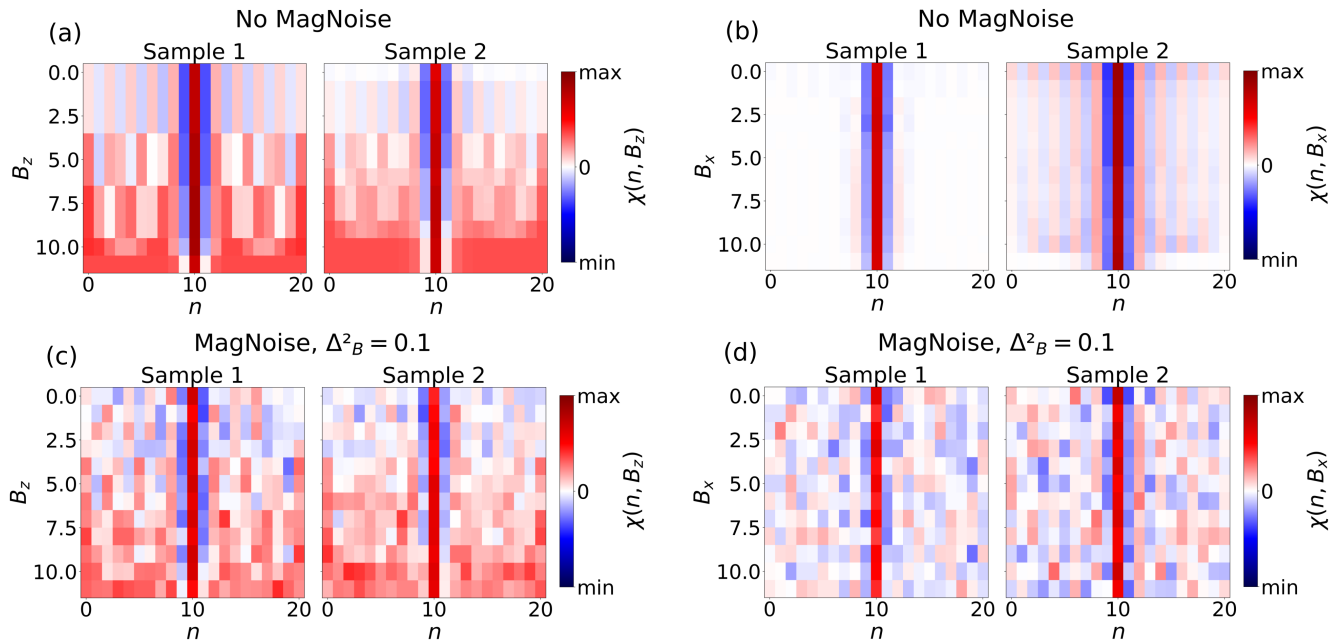


FIG. 5. Evolution of the static spin correlator χ as a function of the external magnetic field B^z (a,c) and the external magnetic field B^x (b,d). Panels (a,b) show the pristine spin correlators, whereas panels (c,d) show the noisy correlators with magnetic noise at $\Delta_B^2 = 0.1$. The evolution of the correlator with the field acts as fingerprint of the many-body system, which the machine learning algorithm leverages to extract the Hamiltonian.

information required to perform Hamiltonian learning. By varying the magnetic field and examining the spin correlators across different sites within the chain, we can generate detailed spatial and magnetic field-dependent data, either by sweeping over the magnetic field in the z -direction (Fig. 5ac) or the x -direction (Fig. 5bd). In Fig. 5a, we show the evolution of the static correlators for different samples, illustrating how the presence of the central spin-1 impurity affects the magnetic excitations across the chain with and without the presence of magnetic noise. Essentially, these images act like fingerprints for specific Hamiltonian parameters, allowing the NN to learn how changes in the magnetic field and spin configurations relate to the underlying Hamiltonian.

Both directions of the magnetic field reflect a non-trivial evolution of the group state, and for our purpose any of those will enable us to perform Hamiltonian learning. In the configuration with B_x , the static spin correlator shows distinct correlation peaks centered around the middle impurity site, which are more symmetric and localized in the noiseless data. When noise is introduced, the clarity of these features decreases but remains discernible. Compared to the B_z configuration, the B_x field produces different correlation patterns, reflecting the anisotropic nature of the system. Both configurations demonstrate that, although noise impacts the sharpness of the data, key features near the impurity site are robust enough to be used for further analysis, such as training neural networks to infer Hamiltonian parameters.

In Fig. 6b, the fidelity of the spin chain model parameters J_2 , J_z , and J_{DM} is presented as a function of the noise level W for the case where the magnetic field B is applied along the z -direction. This comparison includes three scenarios: perfect data, $\Delta_B^2 = 0.05$ and $\Delta_B^2 = 0.1$ magnetic noise level. As observed with the fermionic chain, the fidelity decreases with increasing noise levels. The robustness of J_2 and J_z is evident, maintaining high fidelity even with $\Delta_B^2 = 0.1$ up to $W = 2$. However, J_{DM} shows greater sensitivity to noise, with fidelity dropping significantly as the noise increases, highlighting the stronger impact of noise on learning this parameter. Additionally, magnetic noise broadly diminishes fidelity across all parameters, underscoring its significant effect on model performance.

We show in Fig. 6c the results for the magnetic field B applied along the x -direction. The overall trend remains similar, with fidelity decreasing as noise levels increase. However, the fidelity across parameters in the B_x case shows slightly different sensitivities to noise compared to the B_z case. This difference is likely correlated to the lack of variation in the datasets when B is aligned along the x -axis, suggesting that the reduced variation in the input data could be influencing the model's ability to learn and generalize across different noise levels. Finally, it is worth noting that more advanced machine learning methodologies such as GANs [47, 86] and diffusion models [87, 88] could further improve the efficiency of Hamiltonian learning.

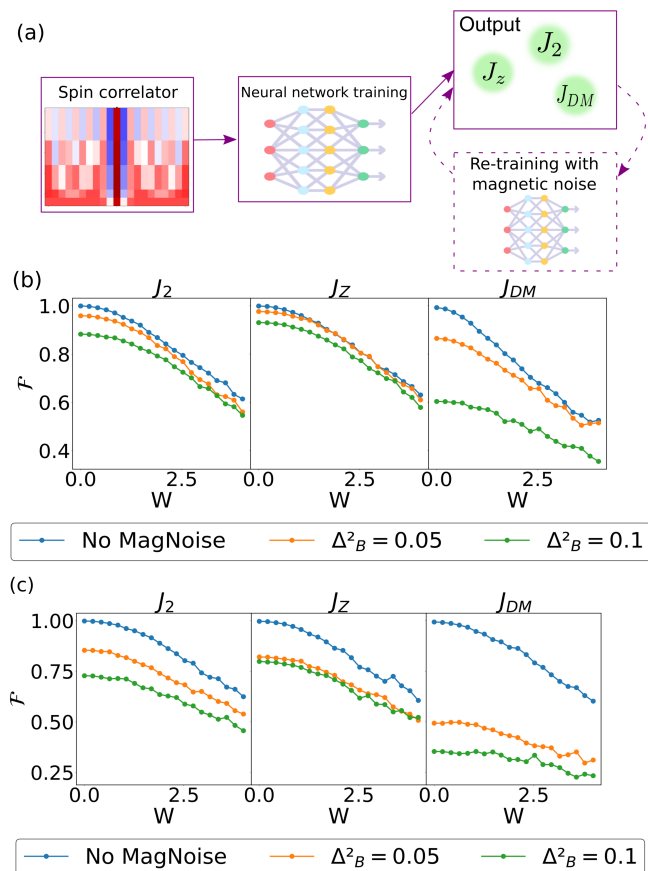


FIG. 6. (a) Hamiltonian learning algorithm of the quantum many-body spin model. Panel (b) shows the fidelity of the spin chain parameters J_2 , J_z , and J_{DM} as a function of the scaling measurement noise W . Panel (b) shows the Hamiltonian learning for a magnetic field in the z direction, and panel (c) for a magnetic field applied in the x direction. Each plot compares the fidelity for data without magnetic noise ($\Delta_B^2 = 0$) and with magnetic noise levels $\Delta_B^2 = 0.05$ and $\Delta_B^2 = 0.1$.

VI. CONCLUSION

Here we presented a machine learning methodology to infer Hamiltonian parameters that leverages the response of a quantum magnet to local impurity perturbations. Our strategy exploits the non-local changes created by localized impurities in a quantum many-body wavefunction, and in particular the dependence of those changes with respect to an externally tunable magnetic field. Our methodology allows extracting both long-range exchange couplings and anisotropic exchange coupling of quantum magnets, effects that often represent a remarkable challenge with conventional methodologies. Our approach offers a powerful method for extracting complex, non-local information from quantum systems, which is often challenging to access through traditional techniques. We showed that this methodology can be carried out in the presence of different noise sources, showing that this approach is robust even in the presence of realistic perturbations. By adapting our methodology to a single particle problem, we showed that this technique enables learning single-particle dispersion, and can be reinterpreted as a machine-learning inspired quasiparticle interference method. Within the single-particle limit, we showed that this technique allows us to extract spin-orbit coupling terms of the electronic structure from a non-polarized observable, an often challenging effect to extract with conventional quasiparticle interference. Our method showcases the powerful synergy between machine learning and quantum many-body methods, in particular, showing how machine learning techniques trained in computational data can be used to learn Hamiltonians from experimental observables. Our results establish a proof of concept to apply this machine-learning methodology to more complex quantum many-body systems, including higher-dimensional quantum magnets and interacting fermionic systems.

ACKNOWLEDGMENTS

We acknowledge financial support from the Academy of Finland Projects Nos. 331342, and 349696, InstituteQ, the Jane and Aatos Erkkö Foundation, and the Finnish Quantum Flagship. We acknowledge the computational resources provided by the Aalto Science-IT project. We thank Tiago Antão, Adolfo Fumega, Rouven Koch, Peter Liljeroth and Robert Drost for useful discussions.

- [1] L. Savary and L. Balents, Quantum spin liquids: a review, *Reports on Progress in Physics* **80**, 016502 (2016).
 [2] C. Broholm, R. J. Cava, S. A. Kivelson, D. G. Nocera, M. R. Norman, and T. Senthil, Quantum spin liquids, *Science* **367**, 10.1126/science.aay0668 (2020).
 [3] M. R. Norman, Colloquium: Herbertsmithite and the search for the quantum spin liquid, *Rev. Mod. Phys.* **88**,

041002 (2016).

- [4] S. Phark, H. T. Bui, A. Ferrón, J. Fernández-Rossier, J. Reina-Gálvez, C. Wolf, Y. Wang, K. Yang, A. J. Heinrich, and C. P. Lutz, Electric-field-driven spin resonance by on-surface exchange coupling to a single-atom magnet, *Advanced Science* **10**, 10.1002/advs.202302033 (2023).

- [5] Y. Wang, Y. Chen, H. T. Bui, C. Wolf, M. Haze, C. Mier, J. Kim, D.-j. Choi, C. P. Lutz, Y. Bae, S.-H. Phark, and A. J. Heinrich, An electron-spin qubit platform assembled atom-by-atom on a surface, *arXiv e-prints*, [arXiv:2108.09880](https://arxiv.org/abs/2108.09880) (2021), [arXiv:2108.09880](https://arxiv.org/abs/2108.09880) [[cond-mat.mes-hall](https://arxiv.org/abs/2108.09880)].
- [6] Y. Wang, Y. Chen, H. T. Bui, C. Wolf, M. Haze, C. Mier, J. Kim, D.-J. Choi, C. P. Lutz, Y. Bae, S. hyon Phark, and A. J. Heinrich, An atomic-scale multi-qubit platform, *Science* **382**, 87 (2023), <https://www.science.org/doi/pdf/10.1126/science.ade5050>.
- [7] D. M. Eigler and E. K. Schweizer, Positioning single atoms with a scanning tunnelling microscope, *Nature* **10.1038/344524a0** (1990).
- [8] K. Yang, W. Paul, W. Paul, S. hyon Phark, P. Willke, Y. Bae, T. Choi, T. Esat, A. Ardavan, A. J. Heinrich, and C. P. Lutz, Coherent spin manipulation of individual atoms on a surface, *Science* **10.1126/science.aay6779** (2019).
- [9] T. S. Seifert, S. Kovarik, D. M. Juraschek, N. A. Spaldin, P. Gambardella, and S. Stepanow, Longitudinal and transverse electron paramagnetic resonance in a scanning tunneling microscope, *Science Advances* **6**, eabc5511 (2020), <https://www.science.org/doi/pdf/10.1126/sciadv.abc5511>.
- [10] S. Baumann, W. Paul, T. Choi, C. P. Lutz, A. Ardavan, A. Ardavan, and A. J. Heinrich, Electron paramagnetic resonance of individual atoms on a surface, *Science* **10.1126/science.aac8703** (2015).
- [11] K. Yang, S.-H. Phark, Y. Bae, T. Esat, P. Willke, A. Ardavan, A. J. Heinrich, and C. P. Lutz, Probing resonating valence bond states in artificial quantum magnets, *Nature Communications* **12**, [10.1038/s41467-021-21274-5](https://doi.org/10.1038/s41467-021-21274-5) (2021).
- [12] S. Loth, S. Baumann, C. P. Lutz, D. M. Eigler, and A. J. Heinrich, Bistability in atomic-scale antiferromagnets, *Science* **335**, 196–199 (2012).
- [13] R. Toskovic, R. van den Berg, A. Spinelli, I. S. Eliens, B. van den Toorn, B. Bryant, J.-S. Caux, and A. F. Otte, Atomic spin-chain realization of a model for quantum criticality, *Nature Physics* **12**, 656–660 (2016).
- [14] A. Spinelli, B. Bryant, F. Delgado, J. Fernández-Rossier, and A. F. Otte, Imaging of spin waves in atomically designed nanomagnets, *Nature Materials* **13**, 782–785 (2014).
- [15] R. Drost, S. Kezilebieke, J. L. Lado, and P. Liljeroth, Real-space imaging of triplon excitations in engineered quantum magnets, *Phys. Rev. Lett.* **131**, 086701 (2023).
- [16] C. Zhao, G. Catarina, J.-J. Zhang, J. C. G. Henriques, L. Yang, J. Ma, X. Feng, O. Gröning, P. Ruffieux, J. Fernández-Rossier, and R. Fasel, Tunable topological phases in nanographene-based spin-1/2 alternating-exchange heisenberg chains, *Nature Nanotechnology* **10.1038/s41565-024-01805-z** (2024).
- [17] H. Wang, P. Fan, J. Chen, L. Jiang, H.-J. Gao, J. L. Lado, and K. Yang, Construction of topological quantum magnets from atomic spins on surfaces, *Nature Nanotechnology* **10.1038/s41565-024-01775-2** (2024).
- [18] M. Aapro, A. Kipnis, J. L. Lado, S. Kezilebieke, and P. Liljeroth, Tuning spinaron and kondo resonances via quantum confinement, *Phys. Rev. B* **109**, 195415 (2024).
- [19] S. Mishra, D. Beyer, K. Eimre, S. Kezilebieke, R. Berger, O. Gröning, C. A. Pignedoli, K. Müllen, P. Liljeroth, P. Ruffieux, X. Feng, and R. Fasel, Topological frustration induces unconventional magnetism in a nanographene, *Nature Nanotechnology* **15**, 22–28 (2019).
- [20] P. Willke, Y. Bae, K. Yang, J. L. Lado, A. Ferrón, T. Choi, A. Ardavan, J. Fernández-Rossier, A. J. Heinrich, and C. P. Lutz, Hyperfine interaction of individual atoms on a surface, *Science* **362**, 336–339 (2018).
- [21] Y. Wang, M. Haze, H. T. Bui, W.-h. Soe, H. Aubin, A. Ardavan, A. J. Heinrich, and S.-h. Phark, Universal quantum control of an atomic spin qubit on a surface, *npj Quantum Information* **9**, [10.1038/s41534-023-00716-6](https://doi.org/10.1038/s41534-023-00716-6) (2023).
- [22] Y. Wang, Y. Chen, H. T. Bui, C. Wolf, M. Haze, C. Mier, J. Kim, D.-J. Choi, C. P. Lutz, Y. Bae, S.-h. Phark, and A. J. Heinrich, An atomic-scale multi-qubit platform, *Science* **382**, 87–92 (2023).
- [23] N. Karjalainen, Z. Lippo, G. Chen, R. Koch, A. O. Fumega, and J. L. Lado, Hamiltonian inference from dynamical excitations in confined quantum magnets, *Phys. Rev. Appl.* **20**, 024054 (2023).
- [24] G. Chen and J. L. Lado, Impurity-induced resonant spinon zero modes in dirac quantum spin liquids, *Phys. Rev. Res.* **2**, 033466 (2020).
- [25] E. J. König, M. T. Randeria, and B. Jäck, Tunneling spectroscopy of quantum spin liquids, *Phys. Rev. Lett.* **125**, 267206 (2020).
- [26] V. Peri, S. Ilani, P. A. Lee, and G. Refael, Probing quantum spin liquids with a quantum twisting microscope, *Phys. Rev. B* **109**, 035127 (2024).
- [27] R. Mazzilli, A. Levchenko, and E. J. König, Drag resistance mediated by quantum spin liquids, *Phys. Rev. B* **108**, 014425 (2023).
- [28] G. Chen and J. L. Lado, Tunable moire spinons in magnetically encapsulated twisted van der waals quantum spin liquids, *Phys. Rev. Res.* **3**, 033276 (2021).
- [29] W.-Y. He and P. A. Lee, Magnetic impurity as a local probe of the $u(1)$ quantum spin liquid with spinon fermi surface, *Phys. Rev. B* **105**, 195156 (2022).
- [30] M. O. Takahashi, W.-H. Kao, S. Fujimoto, and N. B. Perkins, Z_2 flux binding to higher-spin impurities in the Kitaev spin liquid: mechanisms and implications, *arXiv e-prints*, [arXiv:2409.02190](https://arxiv.org/abs/2409.02190) (2024), [arXiv:2409.02190](https://arxiv.org/abs/2409.02190) [[cond-mat.str-el](https://arxiv.org/abs/2409.02190)].
- [31] D. Liu, A. B. Watson, M. Hott, S. Carr, and M. Luskin, Learning the local density of states of a bilayer moiré material in one dimension, *arXiv e-prints*, [arXiv:2405.06688](https://arxiv.org/abs/2405.06688) (2024), [arXiv:2405.06688](https://arxiv.org/abs/2405.06688) [[math-ph](https://arxiv.org/abs/2405.06688)].
- [32] A. D. Tranter, L. Kranz, S. Sutherland, J. G. Keizer, S. K. Gorman, B. C. Buchler, and M. Y. Simmons, Machine learning-assisted precision manufacturing of atom qubits in silicon, *ACS Nano* **10.1021/acsnano.4c00080** (2024).
- [33] J. Benestad, A. Tsintzis, R. S. Souto, M. Leijnse, E. van Nieuwenburg, and J. Danon, Machine-learned tuning of artificial kitaev chains from tunneling spectroscopy measurements, *Phys. Rev. B* **110**, 075402 (2024).
- [34] M. Khosravi, R. Koch, and J. L. Lado, Hamiltonian learning with real-space impurity tomography in topological moiré superconductors, *Journal of Physics: Materials* **7**, 015012 (2024).
- [35] D. van Driel, R. Koch, V. P. M. Sietses, S. L. D. ten Haaf, C.-X. Liu, F. Zatelli, B. Roovers, A. Bordin, N. van Loo, G. Wang, J. C. Wolff, G. P. Mazur, T. Dvir, I. Kulesh, Q. Wang, A. Mert Bozkurt, S. Gazibegovic, G. Badawy, E. P. A. M. Bakkers, M. Wimmer,

- S. Goswami, J. L. Lado, L. P. Kouwenhoven, and E. Greplova, Cross-Platform Autonomous Control of Minimal Kitaev Chains, [arXiv e-prints](#), [arXiv:2405.04596 \(2024\)](#), [arXiv:2405.04596 \[cond-mat.mes-hall\]](#).
- [36] R. Koch, D. van Driel, A. Bordin, J. L. Lado, and E. Greplova, Adversarial hamiltonian learning of quantum dots in a minimal kitaev chain, *Phys. Rev. Appl.* **20**, 044081 (2023).
- [37] G. Carleo, I. Cirac, K. Cranmer, L. Daudet, M. Schuld, N. Tishby, L. Vogt-Maranto, and L. Zdeborová, Machine learning and the physical sciences, *Rev. Mod. Phys.* **91**, 045002 (2019).
- [38] J. Wang, S. Paesani, R. Santagati, S. Knauer, A. A. Gentile, N. Wiebe, M. Petruzzella, J. L. O'Brien, J. G. Rarity, A. Laing, and M. G. Thompson, Experimental quantum hamiltonian learning, *Nature Physics* **13**, 551–555 (2017).
- [39] T. J. Evans, R. Harper, and S. T. Flammia, Scalable Bayesian Hamiltonian learning, [arXiv e-prints](#), [arXiv:1912.07636 \(2019\)](#), [arXiv:1912.07636 \[quant-ph\]](#).
- [40] E. Bairey, I. Arad, and N. H. Lindner, Learning a local hamiltonian from local measurements, *Phys. Rev. Lett.* **122**, 020504 (2019).
- [41] F. Aikebaier, T. Ojanen, and J. L. Lado, Extracting electronic many-body correlations from local measurements with artificial neural networks, *SciPost Phys. Core* **6**, 030 (2023).
- [42] A. Anshu, S. Arunachalam, T. Kuwahara, and M. Soleimanifar, Sample-efficient learning of interacting quantum systems, *Nature Physics* **17**, 931–935 (2021).
- [43] F. Aikebaier, T. Ojanen, and J. L. Lado, Machine learning the kondo entanglement cloud from local measurements, *Phys. Rev. B* **109**, 195125 (2024).
- [44] D. Hangleiter, I. Roth, J. Fuksa, J. Eisert, and P. Roushan, Robustly learning the hamiltonian dynamics of a superconducting quantum processor, *Nature Communications* **15**, 10.1038/s41467-024-52629-3 (2024).
- [45] C. L. Benavides-Riveros, T. Wasak, and A. Recati, Extracting many-body quantum resources within one-body reduced density matrix functional theory, *Phys. Rev. Res.* **6**, L012052 (2024).
- [46] A. Valenti, E. van Nieuwenburg, S. Huber, and E. Greplova, Hamiltonian learning for quantum error correction, *Phys. Rev. Res.* **1**, 033092 (2019).
- [47] R. Koch and J. L. Lado, Designing quantum many-body matter with conditional generative adversarial networks, *Physical review research* [10.1103/physrevresearch.4.033223 \(2022\)](#).
- [48] A. A. Gentile, B. Flynn, S. Knauer, N. Wiebe, S. Paesani, C. E. Granade, J. G. Rarity, R. Santagati, and A. Laing, Learning models of quantum systems from experiments, *Nature Physics* **17**, 837–843 (2021).
- [49] A. Singha, P. Willke, T. Bilgeri, X. Zhang, H. Brune, F. Donati, A. J. Heinrich, and T. Choi, Engineering atomic-scale magnetic fields by dysprosium single atom magnets, *Nature Communications* **12**, 10.1038/s41467-021-24465-2 (2021).
- [50] R. Kubo, Statistical-mechanical theory of irreversible processes. i. general theory and simple applications to magnetic and conduction problems, *Journal of the Physical Society of Japan* **12**, 570–586 (1957).
- [51] J. J. Sakurai and J. Napolitano, *Modern Quantum Mechanics*, 2nd ed. (Cambridge University Press, Cambridge, UK, 2017).
- [52] H. Bruus and K. Flensberg, *Many-Body Quantum Theory in Condensed Matter Physics* (Oxford University Press, Oxford, UK, 2004).
- [53] G. D. Mahan, *Many-Particle Physics* (Springer US, 2000).
- [54] S. Reale, J. Hwang, J. Oh, H. Brune, A. J. Heinrich, F. Donati, and Y. Bae, Electrically driven spin resonance of 4f electrons in a single atom on a surface, *Nature Communications* **15**, 10.1038/s41467-024-49447-y (2024).
- [55] Z. Li, L. Zou, and T. H. Hsieh, Hamiltonian tomography via quantum quench, *Phys. Rev. Lett.* **124**, 160502 (2020).
- [56] A. Czerwinski, Hamiltonian tomography by the quantum quench protocol with random noise, *Phys. Rev. A* **104**, 052431 (2021).
- [57] E. H. Lapasar, K. Maruyama, D. Burgarth, T. Takui, Y. Kondo, and M. Nakahara, Estimation of coupling constants of a three-spin chain: a case study of hamiltonian tomography with nuclear magnetic resonance, *New Journal of Physics* **14**, 013043 (2012).
- [58] X. Chen, Y. Li, Z. Wu, R. Liu, Z. Li, and H. Zhou, Experimental realization of hamiltonian tomography by quantum quenches, *Phys. Rev. A* **103**, 042429 (2021).
- [59] L. Che, C. Wei, Y. Huang, D. Zhao, S. Xue, X. Nie, J. Li, D. Lu, and T. Xin, Learning quantum hamiltonians from single-qubit measurements, *Phys. Rev. Res.* **3**, 023246 (2021).
- [60] F. Wilde, A. Kshetrimayum, I. Roth, D. Hangleiter, R. Sweke, and J. Eisert, Scalably learning quantum many-body Hamiltonians from dynamical data, [arXiv e-prints](#), [arXiv:2209.14328 \(2022\)](#), [arXiv:2209.14328 \[quant-ph\]](#).
- [61] R. Harper, S. T. Flammia, and J. J. Wallman, Efficient learning of quantum noise, *Nature Physics* **16**, 1184–1188 (2020).
- [62] H.-Y. Huang, Y. Tong, D. Fang, and Y. Su, Learning many-body hamiltonians with heisenberg-limited scaling, *Phys. Rev. Lett.* **130**, 200403 (2023).
- [63] E. Flurin, L. S. Martin, S. Hacohe-Gourgy, and I. Siddiqi, Using a recurrent neural network to reconstruct quantum dynamics of a superconducting qubit from physical observations, *Phys. Rev. X* **10**, 011006 (2020).
- [64] W. Yu, J. Sun, Z. Han, and X. Yuan, Robust and efficient hamiltonian learning, *Quantum* **7**, 1045 (2023).
- [65] Y. A. Bychkov and E. I. Rashba, Oscillatory effects and the magnetic susceptibility of carriers in inversion layers, *Journal of Physics C: Solid State Physics* **17**, 6039 (1984).
- [66] G. Bihlmayer, O. Rader, and R. Winkler, Focus on the rashba effect, *New Journal of Physics* **17** (2015).
- [67] A. Manchon, H. C. Koo, J. Nitta, S. M. Frolov, and R. A. Duine, New perspectives for rashba spin-orbit coupling, *Nature Materials* **14**, 871–882 (2015).
- [68] T. Moriya, Anisotropic superexchange interaction and weak ferromagnetism, *Phys. Rev.* **120**, 91 (1960).
- [69] I. Dzyaloshinsky, A thermodynamic theory of “weak” ferromagnetism of antiferromagnetics, *Journal of Physics and Chemistry of Solids* **4**, 241 (1958).
- [70] Y. del Castillo and J. Fernández-Rossier, [Probing spin fractionalization with esr-stm absolute magnetometry \(2023\)](#), [arXiv:2311.15720 \[cond-mat.mes-hall\]](#).
- [71] Y. Liu, W. Yan, H. Zhu, Y. Tu, L. Guan, and X. Tan, Study on bandgap predications of abx3-type perovskites by machine learning, *Organic Electronics* **101**, 106426 (2022).

- [72] M. Rupp, Machine learning for quantum mechanics in a nutshell, *International Journal of Quantum Chemistry* **115**, 1058 (2015), <https://onlinelibrary.wiley.com/doi/pdf/10.1002/qua.24954>.
- [73] M. Braun and J. König, Faraday-rotation fluctuation spectroscopy with static and oscillating magnetic fields, *Phys. Rev. B* **75**, 085310 (2007).
- [74] Z. Yue and M. E. Raikh, Evolution of inhomogeneously broadened spin-noise spectrum with ac drive, *Phys. Rev. B* **91**, 155301 (2015).
- [75] A. V. Poshakinskiy and S. A. Tarasenko, Spin noise at electron paramagnetic resonance, *Phys. Rev. B* **101**, 075403 (2020).
- [76] T. S. Seifert, S. Kovarik, P. Gambardella, and S. Stepanow, Accurate measurement of atomic magnetic moments by minimizing the tip magnetic field in stm-based electron paramagnetic resonance, *Phys. Rev. Res.* **3**, 043185 (2021).
- [77] T. S. Seifert, S. Kovarik, C. Nistor, L. Persichetti, S. Stepanow, and P. Gambardella, Single-atom electron paramagnetic resonance in a scanning tunneling microscope driven by a radio-frequency antenna at 4 k, *Phys. Rev. Res.* **2**, 013032 (2020).
- [78] T. S. Seifert, S. Kovarik, D. M. Juraschek, N. A. Spaldin, P. Gambardella, and S. Stepanow, Longitudinal and transverse electron paramagnetic resonance in a scanning tunneling microscope, *Science Advances* **6**, 10.1126/sciadv.abc5511 (2020).
- [79] K. Yang, W. Paul, F. D. Natterer, J. L. Lado, Y. Bae, P. Willke, T. Choi, A. Ferrón, J. Fernández-Rossier, A. J. Heinrich, and C. P. Lutz, Tuning the exchange bias on a single atom from 1 mT to 10 T, *Phys. Rev. Lett.* **122**, 227203 (2019).
- [80] R. Orús, Tensor networks for complex quantum systems, *Nature Reviews Physics* **1**, 538 (2019).
- [81] T. Choi, W. Paul, S. Rolf-Pissarczyk, A. J. Macdonald, F. D. Natterer, K. Yang, P. Willke, C. P. Lutz, and A. J. Heinrich, Atomic-scale sensing of the magnetic dipolar field from single atoms, *Nature Nanotechnology* **12**, 420–424 (2017).
- [82] F. D. Natterer, K. Yang, W. Paul, P. Willke, T. Choi, T. Greber, A. J. Heinrich, and C. P. Lutz, Reading and writing single-atom magnets, *Nature* **543**, 226–228 (2017).
- [83] T. Esat, D. Borodin, J. Oh, A. J. Heinrich, F. S. Tautz, Y. Bae, and R. Temirov, A quantum sensor for atomic-scale electric and magnetic fields, *Nature Nanotechnology* **19**, 1466–1471 (2024).
- [84] J.-F. Ge, M. Ovadia, and J. E. Hoffman, Achieving low noise in scanning tunneling spectroscopy, *Review of Scientific Instruments* **90**, 10.1063/1.5111989 (2019).
- [85] J. D. Hackley, D. A. Kislitsyn, D. K. Beaman, S. Ulrich, and G. V. Nazin, High-stability cryogenic scanning tunneling microscope based on a closed-cycle cryostat, *Review of Scientific Instruments* **85**, 10.1063/1.4897139 (2014).
- [86] I. J. Goodfellow, J. Pouget-Abadie, M. Mirza, B. Xu, D. Warde-Farley, S. Ozair, A. Courville, and Y. Bengio, *Generative adversarial networks* (2014), [arXiv:1406.2661 \[stat.ML\]](https://arxiv.org/abs/1406.2661).
- [87] J. Sohl-Dickstein, E. A. Weiss, N. Maheswaranathan, and S. Ganguli, *Deep unsupervised learning using nonequilibrium thermodynamics* (2015), [arXiv:1503.03585 \[cs.LG\]](https://arxiv.org/abs/1503.03585).
- [88] J. Ho, A. Jain, and P. Abbeel, Denoising diffusion probabilistic models, in *Advances in Neural Information Processing Systems*, Vol. 33, edited by H. Larochelle, M. Ranzato, R. Hadsell, M. Balcan, and H. Lin (Curran Associates, Inc., 2020) pp. 6840–6851.